Applied Energy 204 (2017) 1240–1250

Contents lists available at ScienceDirect

Applied Energy

journal homepage: www.elsevier.com/locate/apenergy

Non-destructive fast charging algorithm of lithium-ion batteries based on the control-oriented electrochemical model

Zhengyu Chu, Xuning Feng, Languang Lu, Jianqiu Li, Xuebing Han, Minggao Ouyang *

State Key Laboratory of Automotive Safety and Energy, Tsinghua University, Beijing 100084, China

HIGHLIGHTS

- A novel non-destructive fast charging algorithm of lithium-ion batteries is proposed.
- A close-loop observer of lithium deposition status is constructed based on the SP2D model.
- The charging current is modified online using the feedback of the lithium deposition status.
- The algorithm can shorten the charging time and can be used for charging from different initial SOCs.
- The post-mortem observation and degradation tests show that no lithium deposition occurs during fast charging.

ARTICLE INFO

Article history:
Received 29 December 2016
Received in revised form 2 March 2017
Accepted 22 March 2017
Available online 30 March 2017

Keywords:
Lithium-ion battery
Electrochemical model
Lithium deposition
Fast charging
Over-potential observer

ABSTRACT

Fast charging is critical for the application of lithium-ion batteries in electric vehicles. Conventional fast charging algorithms may shorten the cycle life of lithium-ion batteries and induce safety problems, such as internal short circuit caused by lithium deposition at the negative electrode. In this paper, a novel, non-destructive model-based fast charging algorithm is proposed. The fast charging algorithm is composed of two closed loops. The first loop includes an anode over-potential observer that can observe the status of lithium deposition online, whereas the second loop includes a feedback structure that can modify the current based on the observed status of lithium deposition. The charging algorithm enhances the charging current to maintain the observed anode over-potential near the preset threshold potential. Therefore, the fast charging algorithm can decrease the charging time while protecting the health of the battery. The fast charging algorithm is validated on a commercial large-format nickel cobalt manganese/graphite cell. The results showed that 96.8% of the battery capacity can be charged within 52 min. The post-mortem observation of the surface of the negative electrode and degradation tests revealed that the fast charging algorithm proposed here protected the battery from lithium deposition.

1. Introduction

The energy crisis and environmental pollution have aroused interest in clean energy vehicles using electrochemical power sources with lithium-ion batteries worldwide [1]. Fast charging is one of the most critical technologies for application in electrical vehicles [2]. Without fast charging, recharging these batteries takes several hours, and the charging rate is limited to 1 C or less [3] by manufacturers because of concerns relating to safety and durability. Therefore, a non-destructive fast charging algorithm is indispensable for use in electric vehicles.

The fast charging approaches based on empirical strategies have been widely discussed to reduce the charging time. Generally, empirical equations considering voltage or current cut-off values are used to determine the charging current. The most common charging protocol is constant current- constant voltage (CC-CV) charging, which consists of a CC stage followed by a CV stage to avoid overcharge [4]. The rule-based CC-CV charging protocol can be easily implemented in a battery management system (BMS) because of its simple logic and low computational load. However, the charging current and voltage limits for the CC-CV protocol are too conservative, leading to long charging times [5]. To accelerate charging, some fast charging strategies based on CC-CV have been proposed in recent years. For example, a scheme combining multi-stage CC with CV (MCC-CV), as presented in [6], can reduce the charging time. However, choosing the current amplitude and duration of each stage is essential but difficult. Furthermore, an algorithm called the boost charging algorithm, which includes CV-CC-CV charging stages, has been proposed and was

* Corresponding author.
E-mail address: ouymg@tsinghua.edu.cn (M. Ouyang).

http://dx.doi.org/10.1016/j.apenergy.2017.03.111
0306-2619/

Nomenclature

a_s	specific interfacial surface area of particle (m^{-1})
a_i	fitting coefficient of approximation expression of electrolyte concentration
A	electrode plate area (m^2)
b_i	fitting coefficient of approximation expression of equilibrium potential
$c_{s,max}$	maximum lithium concentration in the solid phase (mol m^{-3})
$c_{s,mean}$	mean lithium concentration in the solid phase (mol m^{-3})
$c_{s,surface}$	surface lithium concentration in the solid phase (mol m^{-3})
$D_{e,j}^{eff}$	effective electrolyte ionic diffusivity of electrode "j" or separator (m^2 s^{-1})
F	Faraday constant (C mol^{-1})
i_0	exchange current density (A m^{-2})
I	charge current (A)
$j_{f,j}$	volumetric current density of electrode "j" (A m^{-3})
j_f^s	local volumetric current density of the side reaction (A m^{-3})
j_n	pore wall flux of the particle surface (mol m^{-2} s^{-1})
k	reaction rate constant ($m^{2.5}$ A $mol^{-1.5}$ s^{-1})
r	radial coordinate (m)
R	gas constant (J mol^{-1} K^{-1})
R_s	Particle Radius (m)
$R_{SEI,j}$	resistance of the SEI film of electrode "j" (Ω m^{-2})
t	time (s)
t_+	lithium ion transfer number
T	time constant of the first-order process (s)
$U_{ref,j}$	equilibrium potential of electrode "j" or separator (V)
U_{ref}^s	equilibrium potential of the side reaction (V)

Greek

$\varepsilon_{h,j}$	volume fraction in the phase "h" of electrode "j" or separator
κ	electrolyte phase conductivity (S m^{-1})
κ^{eff}	effective electrolyte phase conductivity ($=\kappa\varepsilon_e^{Brugg}$) (S m^{-1})
κ_D^{eff}	diffusional effective electrolyte phase conductivity ($=2RT\kappa^{eff}(t_+ - 1)/F$) (S m^{-1})
ϕ_h	local potential in the phase "h" (V)
α	charge transfer coefficient
δ_j	thickness of electrode "j" or separator (m)
λ	weighting coefficient of the first-order process term
ω	first-order process term (mol m^{-3})
η_{act}	activation over-potential (V)
η_{sr}	over-potential resulted by side reaction (V)
η_{SEI}	over-potential across the SEI film (V)
σ	solid phase conductivity (S m^{-1})
σ^{eff}	effective solid phase conductivity ($=\sigma\varepsilon_s$) (S m^{-1})

Subscribe

j	electrode, =n or p
h	phase, =s or e
s	solid phase
e	electrolyte phase
n	negative electrode
p	positive electrode
sep	separator

demonstrated to operate with little capacity degradation [7]. However, it does not function when charging from a random state of charge (SOC). Compared with the algorithm containing CC and CV regimes, the linear current decay (LCD) protocol charges the battery with a high rate of current in the initial stage, and subsequently, the current decays linearly to reduce the polarization at the end of charging [8]. Unfortunately, LCD may lead to overcharge, which is detrimental to the battery's safety and life. Similarly, the variant current decay (VCD) protocol starts with a high pulse current, and then, the current decreases nonlinearly according to an empirical equation. VCD can be utilized to charge a battery at a higher rate but also leads to capacity fade and impedance increase at both electrodes [9]. Pulse charging (PC) has the potential to eliminate the polarization effect and increase the speed of charging [10,11], but the current waveform profile is difficult to set properly.

Although fast charging algorithms based on empirical parameters and rules are simple to implement in real vehicle BMSs, they are not based on the battery state and are hence inclined to negatively impact in the battery performance. To improve the reliability and non-destructiveness of fast charging, recent research has begun to address model-based methods. The electrochemical model [5,12–15] and the equivalent circuit model (ECM) [16–19], which are two major varieties of battery models, are reformulated and incorporated in optimal control frameworks to generate optimal charging strategies using various optimal algorithms. The electrochemical model, whose basic framework was first proposed by Newman et al. [20,21], is a mechanistic and comprehensive model based on the first principle describing the electrochemical behavior of the lithium-ion battery. The underlying model consists of four partial differential equations (PDEs) that describe the lithium-ion concentration and charge conservation in the solid and electrolyte phase coordinated with one electrochemical kinetics equation. The lithium deposition status of the battery can be derived by using proper initial boundary conditions. Although the model can generate the real electrochemical status of the battery, it is not suitable for real-time use because of its high computational cost and nonlinearity [22,23]. Compared with mechanistic models, the ECM has intrinsic limits in providing electrochemical information about a battery's internal states. Moreover, most of the aforementioned algorithms are designed for offline use without adaptive functions and, thus, have limited anti-interference capability in a real-time system. To enable monitoring the internal states of a battery online, a computationally inexpensive electrochemical battery model is needed.

The ultimate target of fast charging methods is to minimize both the charging time and the damages caused to the battery. Thermal characteristics [18], mechanical damage to the particles [14] and current and voltage constraints are general concerns during charging. However, lithium deposition might be a more critical problem because it can cause battery degradation and, potentially, critical safety issues. High-rate charging brings irreversible capacity loss, because of lithium deposition induced by high polarization [24]. Lithium metal deposits on the anode surface when the lithium-ion concentration on the particle surface reaches the saturation limit [25,26]. Lithium deposition also occurs under low-temperature or overcharging conditions. The active metallic lithium deposited during charging reacts with the electrolyte, resulting in loss of lithium inventory (LLI) in the battery [27]. The reaction gradually forms new sporadic solid electrolyte interphase (SEI) films, causing the resistance of the battery to increase. The deposited lithium is also likely to become dead lithium once

isolated from the anode basis [28]. In addition to the possible capacity degradation, lithium deposition may lead to further safety problems. For instance, the lithium dendrite may pierce through the separator, thereby triggering an internal short circuit or even thermal runaway [29]. To limit lithium deposition during charging, some fast charging algorithms have been proposed that place constraints on the positive value of anode over-potential [5,13]. Tippmann et al. reported charging current maps under different temperatures, showing the variation of the degree of the lithium deposition as a function of the charging rate and SOC characterized by the degradation factor [30]. The prevailing algorithms, however, cannot be used to observe the anode over-potential online and, thus, best utilize the potential of the battery dynamics.

In this paper, a control-oriented electrochemical model (i.e., a simplified pseudo-two-dimensional [SP2D]) model is introduced. The SP2D model is less computationally complex than the P2D model and can thus be applied for the online observation of lithium deposition at the anode during charging. Based on the lithium deposition status observed by the SP2D model, an online non-destructive fast charging algorithm is further formulated. Two sub-close-loop parts—the anode over-potential observation loop (AOOL) coordinated with the charging current modification loop (CCML)—adjust the time-variant charging current to maintain the observed anode over-potential as close to but still over the lithium deposition potential to strictly suppress lithium deposition. Therefore, this first charging algorithm can shorten the charging time while protecting the battery health. In Section 2, the structure of the SP2D model is introduced. In Section 3, the non-destructive fast charging algorithm is formulated and then simulated by Comsol® linked with Matlab® to demonstrate the ideal performance. In Section 4, a commercial nickel cobalt manganese/graphite (NCM/C) battery is tested to validate the effect of the algorithm for real use.

2. The control-oriented electrochemical model (SP2D model)

In this section, the SP2D model is introduced, and compared with the P2D model in [20]. Table 1 lists all the simplifications of the SP2D model relative to the traditional P2D model. The Li diffusion in the solid phase is simplified by calculating the surface concentration of the solid particle ($c_{s,surface}$) by summing the mean concentration ($c_{s,mean}$) and the estimated difference (w_1 and w_2). $c_{s,mean}$ is derived by iteration at each time step. Additionally, the Li diffusion in the electrolyte phase at the positive electrode, separator, and negative electrode are determined based on the quadratic polynomial fit, respectively. The distribution of potential in the solid/electrolyte phase is simplified using a lumped expression of the volumetric transfer current density ($\bar{j}_f$) to remove the uncontrollability resulting from the PDEs. The distribution of the equilibrium potential U_{ref} in porous electrodes is discretized using 3-order polynomial equations, assuming that the electrode contains 4 nodes in an equidistant distribution, as shown in Fig. 1. Finally, the distribution of the volumetric transfer current density j_f is derived by taking the derivative of the Butler-Volmer Equation, substituting the above expressions, and then evaluating its integral form. In this way, a simplified electrochemical model of the cell dynamics is built for control oriented use.

The detailed simplification approaches are described in [31,32] for readers who may have interest. In these two papers, the SP2D model was shown to have performance similar to that of the traditional P2D model in terms of predicting the cell voltage and estimating the cell internal status but with less computational expense, indicating good potential for real-time application in BMSs.

3. The non-destructive fast charging algorithm

Based on the SP2D model, a non-destructive algorithm for fast charging with inhibited lithium deposition is proposed. Fig. 2 illustrates the primary scheme of the algorithm and the correlations between the parts. The algorithm works with a combination of two close-loop control strategies: AOOL and CCML. In the AOOL, the SP2D model is used for the online observation of the over-potential at the negative electrode/separator interface, where lithium deposition generally occurs first [33]. The real-time cell terminal voltage output U_t measured from the battery and the cell terminal voltage output $\hat{U}_o$ predicted by the SP2D model are compared simultaneously to determine the error between the measured and predicted cell terminal voltage (marked as $\tilde{U}_e$). By taking the estimation error of the cell terminal voltage $\tilde{U}_e$ as a feedback signal, the internal states of the SP2D model can be adjusted automatically, ensuring that the SP2D model can track the dynamics of the real battery. In this way, the anode over-potential can be predicted accurately. In the CCML, the difference between the observed anode over-potential $\hat{\eta}_{sr}$ and predetermined threshold potential η_{thr}, which is termed $\Delta\eta$, is used as an additional feedback signal to tune the charging current automatically, ensuring that the observed anode over-potential is as close to the threshold potential as possible during charging. The fast charging algorithm with two closed loops shown using purple and blue blocks, is shown in Fig. 2.

The AOOL and CCML will be sequentially elucidated in Section 3.1 and Section 3.2. Simulation results are shown to demonstrate the advantages of the AOOL and CCML strategies and were obtained by using Comsol Livelink® live-linked with Matlab®. The

Table 1
The simplifications in the SP2D model compared with the P2D model.

Cell dynamics	Traditional P2D model Basic equations	Simplifications in the SP2D model Simplified equations
Solid phase Li diffusion	$\frac{\partial c_s}{\partial t} = \frac{D_s}{r^2}\frac{\partial}{\partial r}\left(r^2\frac{\partial c_s}{\partial r}\right)$	$c_{s,mean}(t_{k+1}) = c_{s,mean}(t_k) - 3\frac{j_n}{R_s}(t_{k+1}-t_k)$ $c_{s,surface}(t_{k+1}) = c_{s,mean}(t_k) + w_1(t_k) + w_2(t_k)$
Electrolyte phase Li diffusion	$\frac{\partial}{\partial t}\varepsilon_e c_e = \frac{\partial}{\partial x}\left(D_e^{eff}\frac{\partial}{\partial x}c_e\right) + (1-t_+)\frac{j_f}{F}$	$c_e(z,t) = \begin{cases} f_n(z,t) = a_1 z^2 + a_2 & 0 \le z \le \delta_n \\ f_{sep}(z,t) = a_3 z^2 + a_4 z + a_5 & \delta_n \le z \le \delta_n + \delta_{sep} \\ f_p(z,t) = a_6(L-z)^2 + a_7 & \delta_n + \delta_{sep} \le z \le L \end{cases}$
Solid phase: charge conservation	$\frac{\partial}{\partial x}\left(\sigma^{eff}\frac{\partial}{\partial x}\phi_s(x,t)\right) - j_f(x,t) = 0$	$\frac{\partial}{\partial x}\phi_s(x,t) \approx \frac{I(t)}{\sigma^{eff}A}\left(\frac{x}{\delta_n} - 1\right)$
Electrolyte phase: charge conservation	$j_f(x,t) + \frac{\partial}{\partial x}\left(\kappa^{eff}\frac{\partial}{\partial x}\phi_e(x,t)\right) + \frac{\partial}{\partial x}\left(\kappa_D^{eff}\frac{\partial}{\partial x}\ln c_e(x,t)\right) = 0$	$\frac{\partial}{\partial x}\phi_e(x,t) \approx -\frac{2RT(t_+-1)}{F}\frac{\partial}{\partial x}\ln c_e(x,t) - \frac{I(t)}{A\delta_n\kappa^{eff}}x$
Equilibrium potential	Depends on local Li concentration $U_{ref} = OCV\left(\frac{c_{s,mean}}{c_{s,max}}\right)$	Simplified using polynomial equation $U_{ref} = b_3x^3 + b_2x^2 + b_1x + b_0$
Volumetric transfer current density	Butler-Volmer Equation $j_f(x,t) = 2a_s i_0 \sinh\left(\frac{\alpha F}{RT}\eta_{act}(x,t)\right)$	$j_f = \frac{1}{p}\left(-\frac{I}{\sigma^{eff}A}x + \left(\frac{1}{\kappa^{eff}} + \frac{1}{\sigma^{eff}}\right)\frac{I}{A\delta_n}\frac{x^2}{2} + \frac{2RT(t_+-1)}{F}\ln c_e - U_{ref}\right) + const$

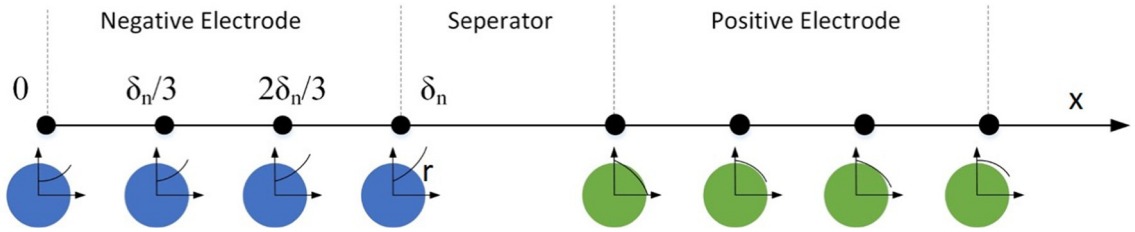

Fig. 1. The 4-node simplification at the battery electrode for the SP2D model.

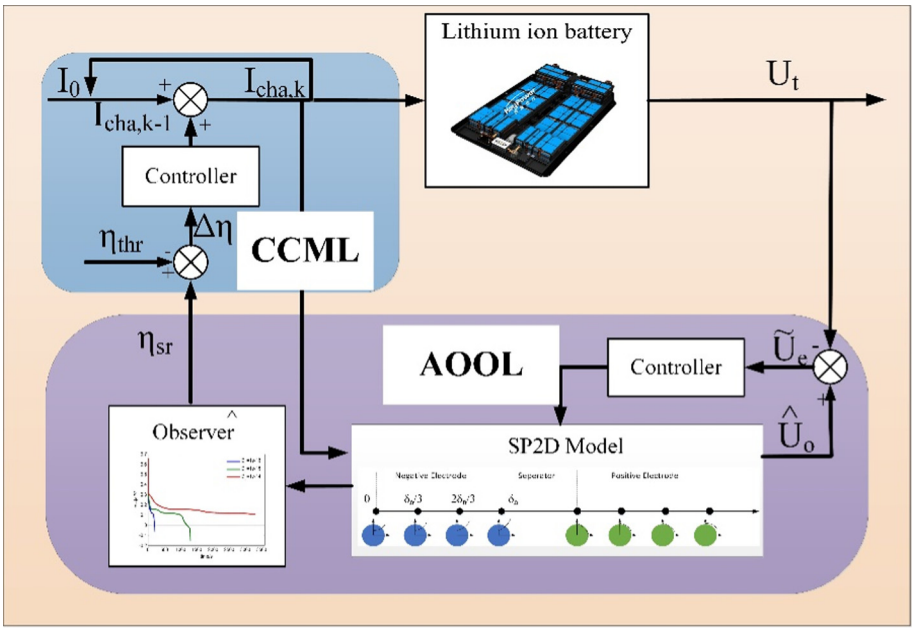

Fig. 2. Fast charging algorithm control scheme.

P2D model is calculated in Comsol Multiphysics® with numerical PDE functions and, solved using a "virtual battery" to give the "measured" terminal voltage, anode over-potential and other battery states, and the SP2D model is simultaneously simulated in Matlab® to serve as the online observer.

3.1. The AOOL

To facilitate the design of the observer, the information needed about the battery electrochemical dynamics is discussed here. The over-potential of the side reaction, which is mainly caused by unexpected polarization resulting from charge-transfer dynamics and diffusion dynamics, is defined by Eq. (1)

$$\eta_{sr}(x,t) = \phi_s(x,t) - \phi_e(x,t) - U^s_{ref}(x,t) - \frac{R_{SEI}}{a_s} j^s_f(x,t) \tag{1}$$

where ϕ_s and ϕ_e are the potentials in the solid and electrolyte phases, respectively. U^s_{ref} represents the equilibrium potential of the side reaction, and j^s_f is the local volumetric current corresponding to the rate of the interfacial side reaction. The lithium deposition reaction starts when the value of U^s_{ref} is lower than 0V. Additionally, j^s_f maintains a value of 0A/m^3 until the side reaction occurs [34]. Therefore, without lithium deposition, Eq. (1) can be simplified to Eq. (2)

$$\eta_{sr}(x,t) = \phi_s(x,t) - \phi_e(x,t) \tag{2}$$

The solution to $\phi_s - \phi_e$ in the SP2D model has been reported in [31], hence, the η_{sr} at the negative electrode/separator interface, where $x = \delta_n$, is calculated in the form of Eq. (3)

$$\eta_{sr}(\delta_n) = U_{ref,n}(\delta_n) + \frac{R_{SEI,n}}{a_{s,n}} j_{f,n}(\delta_n) + \frac{RT}{\alpha F} \operatorname{arcsinh}\left(\frac{j_{f,n}(\delta_n)}{2a_{s,nn} i_{0,n}}\right) \tag{3}$$

The negative electrode/separator interface $\eta_{sr}(\delta_n)$ is chosen as the focus of the observation of the electrochemical model because it is the first indicator of lithium deposition on the anode surface. Specifically, the definite criterion for lithium deposition is $\eta_{sr}(\delta_n) < 0$ V. For porous negative electrodes made of other materials, such as $Li_4Ti_5O_{12}$ and Si/C, the anode over-potential distribution and lithium deposition criteria is also available because of their similar reaction mechanisms.

Based on the electrochemical dynamics theory proposed above, the AOOL was built to observe the $\eta_{sr}(\delta_n)$. For real-time use, failing to estimate the initial status of the battery and uncertainty regarding the disturbance of the algorithm will cause significant estimation errors. To avoid this problem, the close-loop structure is designed to force the internal states of the SP2D model to track the real status of the battery. In [31], the calculation procedures used to predict the terminal voltage are shown in detail, using preset parameters in the model. Based on the above discussion, the lithium-ion battery is regarded as a non-linear control system, and its discrete-time state-space equation has the form

$$\begin{aligned} \mathbf{x}_k &= f_k(\mathbf{x}_{k-1}, \mathbf{u}_k) \\ \mathbf{z}_k &= g_k(\mathbf{x}_k, \mathbf{u}_k) \end{aligned} \tag{4}$$

Herein, the model state vector $\mathbf{x}_k$ comprises the mean solid concentration $c_{s,mean}$ at 8 nodes in both the negative and positive electrode. The input variable $\mathbf{u}_k$ is the charging current I_k. The output

signal variable $\mathbf{z}_k$ is the terminal voltage $V_{t,k}$. At time k, the state $\mathbf{x}_k$ is iteratively computed from $\mathbf{x}_{k-1}$ and $\mathbf{u}_k$ via function f_k. Similarly, the output variable $\mathbf{z}_k$ is computed from $\mathbf{x}_k$ and $\mathbf{u}_k$ via function g_k. Note that f_k and g_k are time-varying functions with no simple explicit form because of their high nonlinearity. Despite its complexity, the discrete-time state-space equation can observe model state $\mathbf{x}_k$. The state observer is designed in the form of Eq. (5).

$$\hat{\mathbf{x}}_k = f_k(\hat{\mathbf{x}}_{k-1}, \mathbf{u}_k) + h(\mathbf{z}_k - \hat{\mathbf{z}}_k) \tag{5}$$

where states $\hat{\mathbf{x}}_k, \hat{\mathbf{x}}_{k-1}$ and output $\hat{\mathbf{z}}_k$ denote the estimated variables. Function h is the feedback gain function used to revise the observation error. More specifically, h is computed as the difference between output variable $\mathbf{z}_k$ and $\hat{\mathbf{z}}_k$, where $\hat{\mathbf{z}}_k = g_k(\hat{\mathbf{x}}_k, \mathbf{u}_k)$, via the function h. Function h is computed by multiplying a gain matrix $\boldsymbol{C}$ and $L(\tilde{\mathbf{z}}_k)$, which is a function of $\tilde{\mathbf{z}}_k$, where $\tilde{\mathbf{z}}_k = (\mathbf{z}_k - \hat{\mathbf{z}}_k)$, as shown in Eq. (6). The principle of proportional-integral-derivative (PID) control is applied to generate function $L(\tilde{\mathbf{z}}_k)$, in which the terms $k_{\mathrm{p,state}}$, $k_{\mathrm{i,state}}$ and $k_{\mathrm{d,state}}$ are introduced to diminish the observation error. The proper selection of the parameters of matrix $\boldsymbol{C}$ and function $L(\tilde{\mathbf{z}}_k)$ will force the observed state $\hat{\mathbf{x}}_k$ to track the real state $\mathbf{x}_k$ as far as possible. Given state $\hat{\mathbf{x}}_k$, the anode over-potential can be computed by Eq. (3).

$$\begin{aligned} h &= \mathbf{C}L(\tilde{\mathbf{z}}_k) \\ L(\tilde{\mathbf{z}}_k) &= k_{\mathrm{p,state}}\tilde{\mathbf{z}}_k + k_{\mathrm{i,state}}\sum_{i=1}^{k}\tilde{\mathbf{z}}_i + k_{\mathrm{d,state}}(\tilde{\mathbf{z}}_k - \tilde{\mathbf{z}}_{k-1}) \\ \mathbf{C} &= [c_1, c_2, c_3, c_4]^T \end{aligned} \tag{6}$$

Fig. 3 compares the observation of the anode over-potential $\hat{\eta}_{\mathrm{sr}}$ of a virtual battery simulated in Comsol under dynamic stress test (DST) conditions using the AOOL algorithm and open-loop algorithm. The cell voltage and anode over-potential of the virtual battery are acquired from the P2D model solved by Comsol. Between the virtual battery and the SP2D model, all the parameters are identical except for the initial state of the solid mean concentration $c_{\mathrm{s,mean}}$ at 8 nodes. For the algorithm without AOOL, $\tilde{U}_o$ and $\hat{\eta}_{\mathrm{sr}}$ evidently deviate from the real status of the battery during DST profiling, whereas the state is corrected within 30 s when the AOOL is used.

3.2. The CCML

Section 3.1 states that the AOOL increases the reliability of the anode over-potential $\hat{\eta}_{\mathrm{sr}}$ for online fast charging control. The CCML was created to automatically adjust the charging current I_{cha} according to the gap between the observed anode over-potential $\hat{\eta}_{\mathrm{sr}}$ and the preset threshold potential η_{thr} during charging. A larger gap between $\hat{\eta}_{\mathrm{sr}}$ and η_{thr} causes I_{cha} to increase at a higher rate. The specific change of I_{cha} is computed by a PID controller as shown in Eq. (7)

$$\Delta I_{\mathrm{cha},k} = k_{\mathrm{p,current}}\eta_{\mathrm{gap},k} + k_{\mathrm{i,current}}\sum_{i=1}^{k}\eta_{\mathrm{gap},i} + k_{\mathrm{d,current}}(\eta_{\mathrm{gap},k} - \eta_{\mathrm{gap},k-1}) \tag{7}$$

where $\eta_{\mathrm{gap}} = \hat{\eta}_{\mathrm{sr}} - \eta_{\mathrm{thr}}$ and the terms $k_{\mathrm{p,current}}$, $k_{\mathrm{i,current}}$ and $k_{\mathrm{d,current}}$ are PID constants that are preset in the controller. Fig. 4(a)–(d) demonstrates a case of charging from SOC = 0 using the fast charging algorithm with both AOOL and CCML. A deviation between the initial state of the virtual battery and the SP2D model is preset to examine the validity of the algorithm. The error of the cell voltage is eliminated swiftly at the beginning of charging with the AOOL, as shown in Fig. 4(a). Additionally, for the anode over-potential $\hat{\eta}_{\mathrm{sr}}$, the results of the virtual battery and model are in good agreement, as shown in Fig. 4(b) and (d).

The charging current is initiated with a current density of 17 A/m^2, which is the normalized current density for a 1 C charging rate. Although higher initial value of the current density can further shorten the charging time, the current is limited here to reduce the heat generation considering the extremely high resistance that occurs at lower SOC [18]. Because $\hat{\eta}_{\mathrm{sr}}$ is still a long distance from η_{thr}, the current desity increases from 1 C to a maximum of approximately 7 C within approximately 180 s as depicted in Fig. 4. To maintain the anode over-potential $\hat{\eta}_{\mathrm{sr}}$ as close to η_{thr} as possible, a lower rate of current density is accommodated at higher SOCs. Therefore, the charging current decreases gradually to keep $\hat{\eta}_{\mathrm{sr}}$ close to η_{thr}. Under these conditions, charging is finished in 10 min and reaches 95.3% of the full capacity.

To avoid overshooting when $\hat{\eta}_{\mathrm{sr}}$ is less than 0 V, the threshold potential η_{thr} is set with a substantial safety margin (i.e., 5 mV in Fig. 4(b)). The unexpected overshoot of $\hat{\eta}_{\mathrm{sr}}$ may result from the use of improper parameters in the PID controller, the current density distribution in a cell plate and the inconsistency of batteries in a battery pack. The improper controller settings can be solved by adjusting the parameters to avoid overshoot. The effects of unequal current distribution and battery inconsistency are relatively significant because lithium deposition may occur in some areas that experience harsh conditions, such as the boundary or winding area, whereas others are remain protected. This situation represents a trade-off: A larger safety margin leads to a lower possibility of lithium deposition but a longer charging time. How to select the threshold potential while balancing the risk of lithium deposition and the charging time will be discussed in Section 4.3.

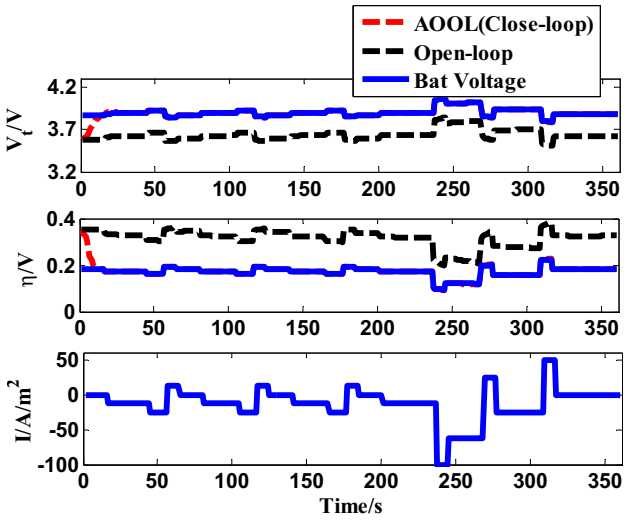

Fig. 3. Comparison between AOOL (close-loop) and open-loop under DST cycle.

3.3. Fast charging from an arbitrary SOC

The fast charging algorithm when battery charging starts from an arbitrary SOC was also evaluated. Fig. 5 shows the cell voltage, anode over-potential, and charging current profiles of the virtual battery with initial open-circuit voltages (OCVs) of 3.73 V and 3.86 V using the fast charging algorithm. Although deviation is preset in the initial state, the SP2D model quickly adapts itself to track the cell voltage, and as result, the observed anode over-potential is close to the real status of the virtual battery. The error in the cell voltage is eliminated within 40 s and 50 s after starting for initial OCVs of 3.73 V and 3.86 V, as shown in Fig. 5(a) and (d). Different initial SOCs exert a similar influence on the charging current: A higher initial SOC leads to a lower current (i.e., the maximum currents rates during charging were 5.4 C and 4.7 C for the cases above, respectively, as shown in Fig. 5(c) and (e)).

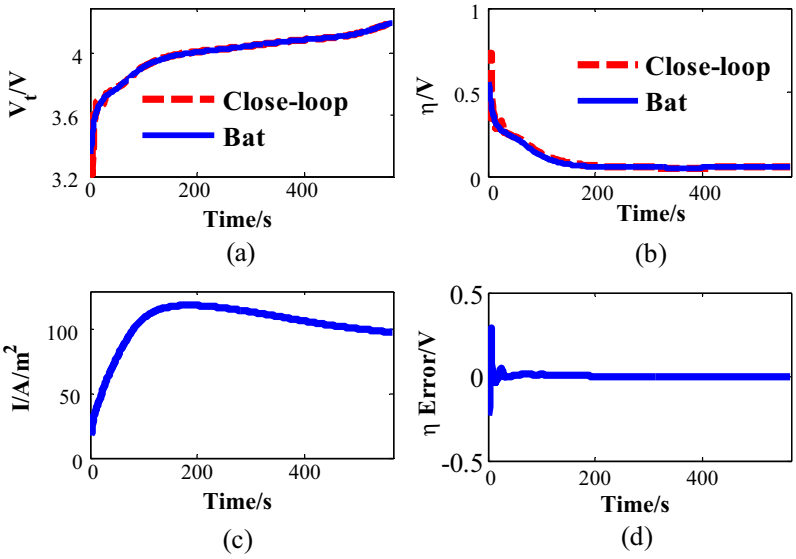

Fig. 4. Charging profiles using the charging current modification loop algorithm.

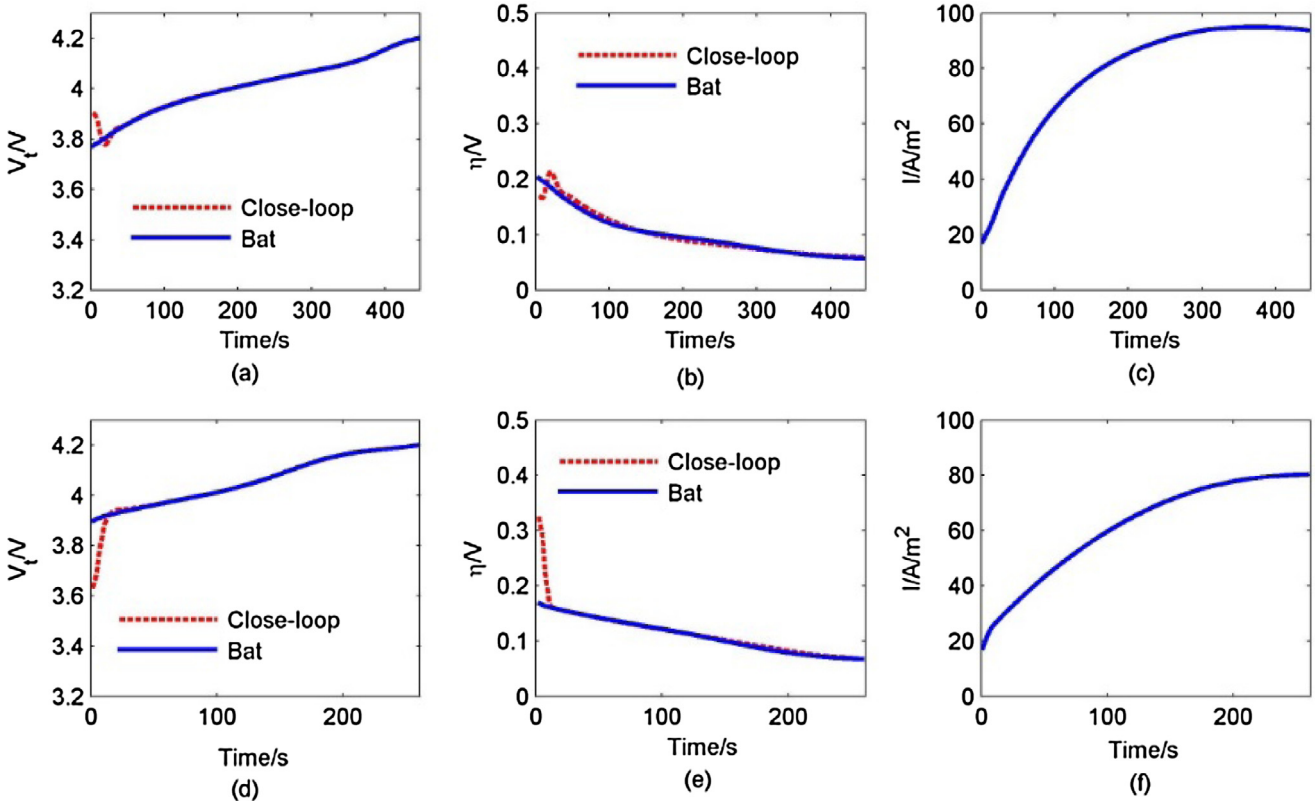

Fig. 5. Profiles of charging from different initial OCV: (a)–(c) 3.73 V, (d)–(f) 3.86 V.

4. Applying the fast charging algorithm to a commercial lithium-ion battery: experimental validation

The test results obtained by applying the fast charging algorithm to a large-format commercial lithium-ion battery with an incorporated reference electrode are presented in this section. The commercial pouch cells consisted of NCM/graphite electrodes. The nominal capacity was 40 A h, and the voltage range was 2.8–4.2 V. To construct a three-electrode cell, the oxidation was removed from a 25-μm-diameter copper wire by acid washing, and the wire was then placed on the surface of the anode/separator interface. The copper wire was wrapped with insulating tape to avoid short circuit. After the fresh was subjected to SEI formation cycles, lithium was electroplated onto the copper wire using a constant deposition current. To form a uniform lithium layer, the deposition current (50 μA for 1 h), was first applied between the copper wire and positive electrode and then between the copper wire and the negative electrode. Subsequently, the three-electrode cells were subjected to a performance test followed by a series of fast charging experiments. An Arbin Battery Testing

Instrument BT-5HC was utilized to charge and discharge the cells, and a temperature chamber was used to maintain a constant temperature during the tests. The schematic of the fast charging test platform is shown in Fig. 6. To meet the time-variable current requirement of the proposed algorithms, the software platform was specially designed for real-time signal processing and transmission.

4.1. Calibration of the SP2D model

The parameters used in the SP2D model were calibrated by CC charging at different charging rates ranging from 0.2 C (8 A) to 5 C (200 A) at room temperature using the three-electrode cells. Within this current range, the model is sufficient for further application of the fast charging algorithm because the maximum charging current in real use is estimated to be lower than 5 C.

The battery was first charged to 4.2 V at a CC and then discharged to 2.8 V at a CC. Then, the battery was charged again at a CC until all of the charging rates were tested. Fig. 7 compares the model and experimental results for the full-cell voltage and anode over-potential; the model prediction is in good agreement with the experimental data. Indeed, the calibrated model parameters were mainly initial surface concentration of particles in the anode and cathode, respectively. The material property parameters, such as σ, κ, and δ etc., can be obtained from the manufacturer. The calibration is terminated when the mean relative error between the model and experimental terminal voltage is lower than 1%, and the mean absolute error between the model and experimental anode over-potential is lower than 10 mV.

4.2. The fast charging results and post-mortem observation of lithium deposition

After the model validation, three-electrode 40 A h batteries were prepared following the same ways, for the fast charging test. Figs. 8 and 9 show the fast charging test results obtained using different initial SOCs (0%, 20% and 40%). Before the fast charging algorithm was undertaken, the battery was first discharged with a CC of 1 C (40 A) to 2.8 V and then pre-charged to the initial SOC (0%, 20% or 40%) with a CC of 1 C (40 A). After resting for 3 h, the battery

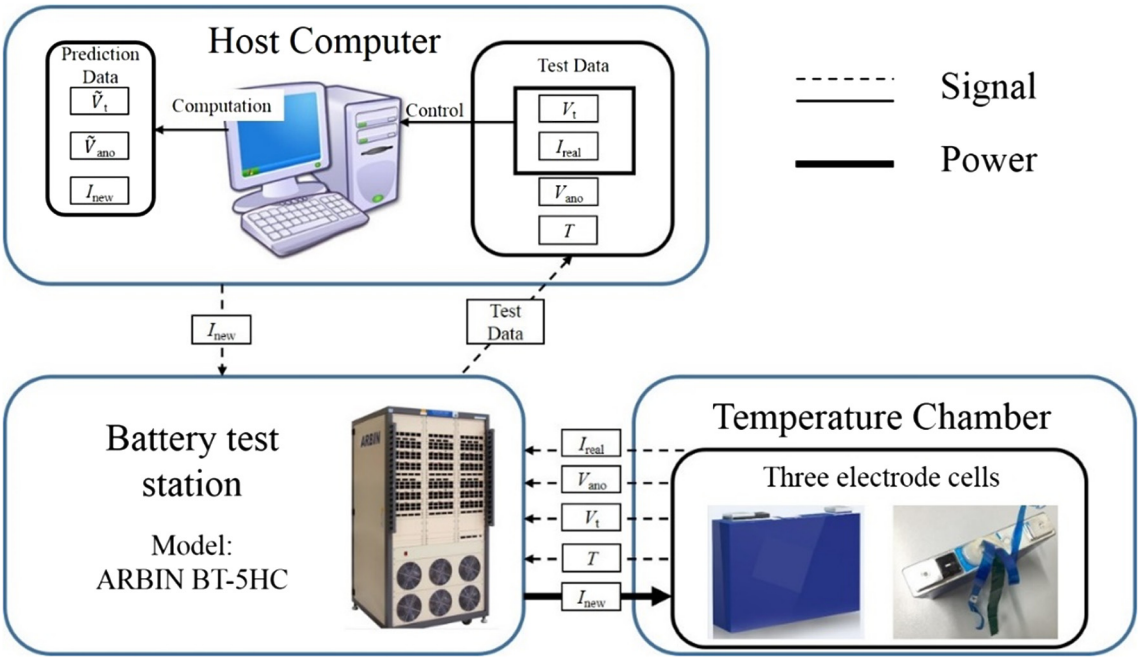

Fig. 6. Fast charging test platform scheme.

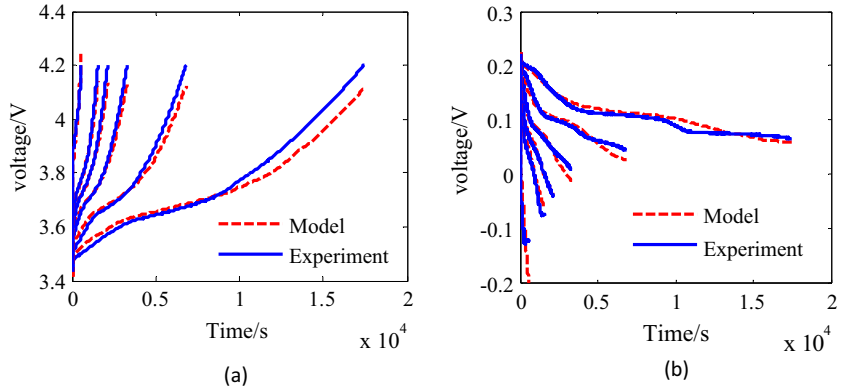

Fig. 7. Model calibration of the SP2D model by experimental charging data at C-rates of 0.2C, 0.5C, 1C, 1.5C, 2C, 5C with the three electrode cell: (a) cell terminal voltage (b) anode over-potential.

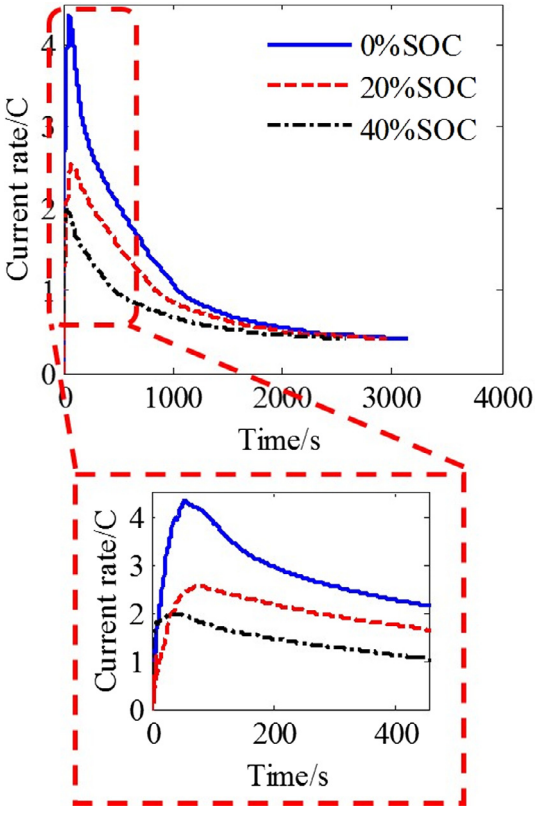

Fig. 8. The current profiles of the fast charging initiated from different SOCs.

was then charged by the proposed fast charging algorithm. The parameters set in the AOOL and CCML controllers are listed in Table 2.

Fig. 8 shows that similar current profiles were obtained during fast charging from initial SOCs of 0%, 20%, and 40%. All the profiles display similar patterns over time: The charging current is quickly increased maximized within 100 s, followed by a long-term decrease. Despite the different initial SOCs, the current similarly levels off to a plateau at a low C-rate (approximately 0.4 C [16A]). The convergence of the charging current can be explained by the fact that the cells converge to the similar statuses at the end of charging.

Table 2
The parameters set in the fast charging algorithm.

Controller	Paramters	Values
AOOL	$k_{p,state}$	500
	$k_{i,state}$	400
	$k_{d,state}$	0
CCML	$k_{p,current}$	20
	$k_{i,current}$	0
	$k_{d,current}$	50
	η_{thr}/mV	30

Table 3 illustrates some characteristics of the fast charging algorithm with different initial SOCs. The average current rate can be computed by dividing the charged capacity by the total charging time. Here, 3148 s (52.5 min) are required for the battery to be charged to 38.7 A h (i.e., 96.8% of the full capacity). Moreover, only 1891 s (31.5 min) are needed to charge to 80% SOC (32 A h) because there is sufficient space for the anode over-potential from 0 V to avoid lithium deposition at the beginning; thus, a higher current rate can be realized. In real-time use, the current limitation can be set easily based on the requirement of the power grid load.

The cell terminal voltage and anode over-potential profiles are illustrated in Fig. 9. The charging tests with initial SOCs of 0%, 20%, and 40% are shown in blue, red, and black lines, respectively. The dashed and solid lines denote the model prediction and test results, respectively. On the one hand, the terminal voltage increases spontaneously to approximately 3.8 V at the beginning of charging and then exhibits moderate growth. On the other hand, the anode over-potential approaches the threshold potential (25 mV) under control and is subsequently maintained as close to the threshold potential as possible. The charging speed can be increased because substantial gaps remain between the observed anode over-potential and the threshold potential. The optimization of the controller to meet the requirements of faster charging will be addressed in our future research.

To illustrate the advantages of the proposed algorithms, experimental data were collected using the universal voltage protocol (UVP) [18], multistage constant current (MCC) [35] and conventional CC-CV and are included for comparison in Fig. 10. Clearly, the current profile of the proposed algorithm resembles that of the UVP algorithm. Indeed, the current increases from the beginning of the charging process until it reaches its maximum, and then gradually decays. In contrast, the proposed algorithm, has a higher maximum current and the current increases at a faster rate; there-

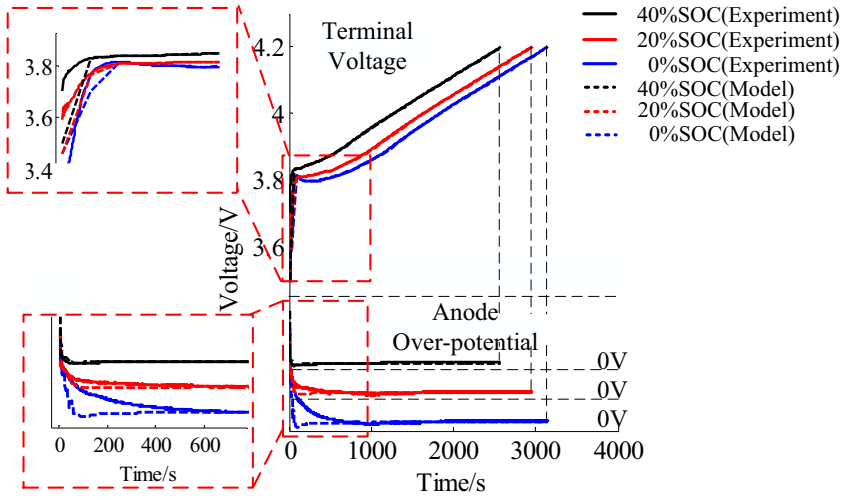

Fig. 9. The voltage profiles of the fast charging algorithm with different initial SOCs.

fore, a large part of the capacity is charged in the beginning. The online observation of lithium deposition enables this algorithm to take full advantage of the dynamic capability of the battery and, thus, generate the optimal current profile. Table 4 shows the experimental data of the charging time, charged capacity, and lithium deposition status obtained using the discussed charging algorithms described in this section and in references. According to Table 4, the proposed algorithm has the fastest charging speed and is the only one that can inhibit lithium deposition. Although the charged capacity of the algorithm is less than those of the CC-CV and UVP protocols, 96.8% is suitable for practical applications.

Table 3
Characteristics of the fast charging algorithm from different initial SOCs.

SOC	Charging time/s	Charged capacity/Ah	Average current (A)	Maximum current/A
0%	3148	38.7	41.3A(1.0C)	174.7A(4.4C)
20%	2954	29.7	37.0A(0.9C)	101.8A(2.5C)
40%	2580	21.4	27.9A(0.7C)	79.7A(2.0C)

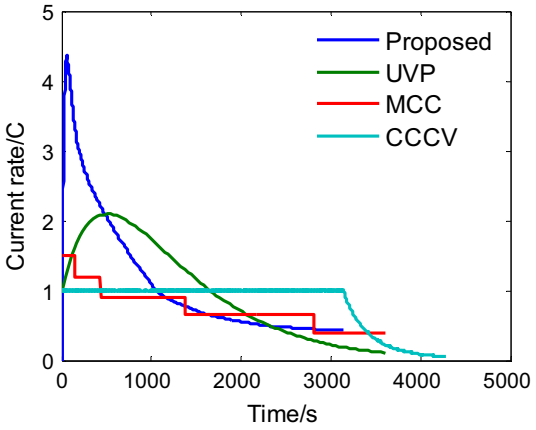

Fig. 10. Charging protocols of the proposed and the former algorithms.

Table 4
Characteristics data of the proposed and the previous charging algorithms.

Charging algorithm	Charging time/s	Charged capacity/%	Lithium deposition
Proposed	3148	96.8%	No
UVP	3600	99.5%	/
MCC	3614	92.1%	/
CC-CV	4278	99.8%	Yes

A post-mortem observation was conducted by comparing the surface morphologies of the negative electrode after CC charging and charging using the proposed fast charging algorithm. Two cells were subjected to five cycles of the two distinct charging strategies at room temperature. To facilitate comparison, the total charging time for the two charging strategies was identical. More specifically, in each cycle, Cell A was charged to 4.2 V with a CC of 1.15 C (46 A), whereas Cell B was charged by the fast charging algorithm, as shown by the solid line in Fig. 8. Both charging processes were followed by a 1 C discharge to 2.8 V. Cells A and B were then disassembled in a drying room for visual inspection of the negative electrode surface. Fig. 11(a) reveals some greyish white regions, which are marked by red rectangles, on the surface of the negative electrode, indicating lithium deposition. During charging, plated metallic lithium tends to appear at the edges and corners. This phenomenon may occur because the higher current density leads to more severe conditions for lithium deposition in these regions. In contrast, Fig. 11(b) shows that the surface of the negative electrode

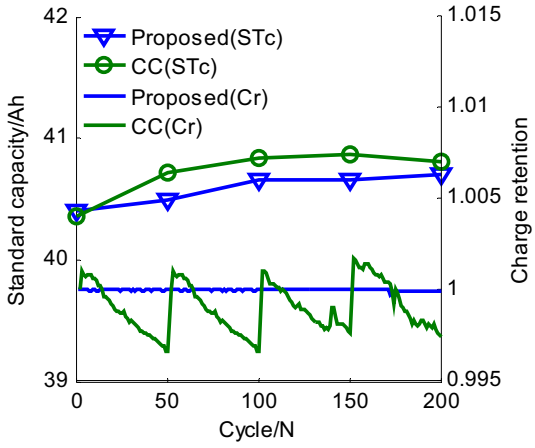

Fig. 12. Standard capacity and charge retention during the cycle degradation test using the proposed and CC charging protocols.

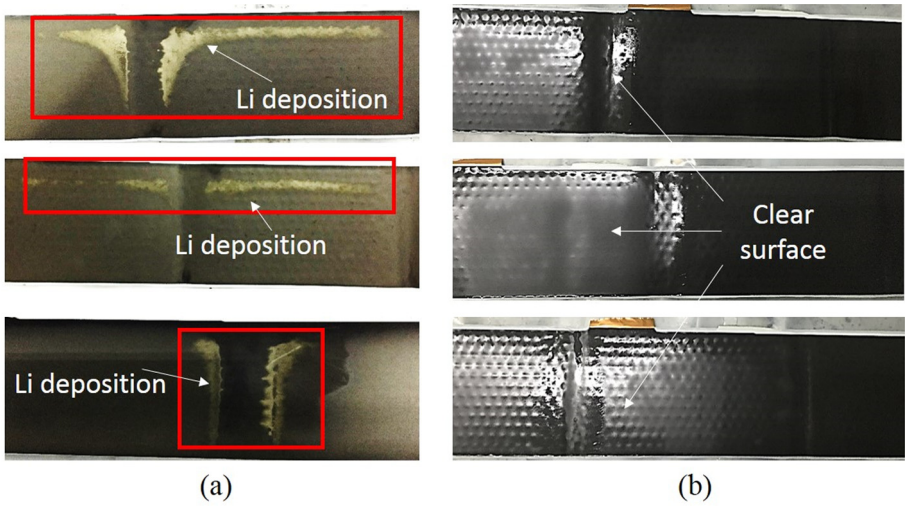

Fig. 11. The surface inspection of the anode after cycles: (a) constant current charging (b) fast charging.

Table 5
Comparison of the fast charging algorithm with different threshold potentials.

Threshold potential/mV	Charging time/s	Charged capacity/Ah	Average current/A	Maximum current/A	Minimum anode over-potential/mV
20	2579	37.5(93.8%)	48.9(1.2C)	176.7(4.4C)	17
30	3148	38.7(96.8%)	41.3(1.0C)	174.7(4.4C)	20
40	3824	38.0(95.0%)	33.4(0.8C)	159.1(4.0C)	24

of Cell B is black and clean, indicating that no lithium deposition occurred during the fast charging.

A total of 200 cycles were conducted using the proposed algorithm and the 1.15 C CC charging protocol. The standard capacity (STc) and charge retention (Cr) are illustrated in Fig. 12. The STc is obtained from the average discharge capacity of the STc test, which comprises 1/3 C charging and 1 C discharging repeated 3 times (at 50 cycle intervals). The Cr is defined as the charge capacity during each cycle. The STc of the proposed algorithm was very steady, whereas the STc of the CC charging protocol tended to decrease after 150 cycles. The Cr of the proposed algorithm remained almost constant during cycling, as shown by the Cr data, indicating that the charge capability is stable and that the polarization does not increase. In contrast, the Cr obtained during CC charging exhibited a continuous decrease during each 50—cycle tests, which results in increased battery polarization. The increase of the internal resistance caused by lithium deposition contributed to the increased battery polarization. Thus, the proposed algorithm can protect batteries from lithium deposition during fast charging cycles. Note that for CC charging, lithium deposition cannot be directly observed based on the actual capacity change because deposited lithium reversibly diffuses into the graphite during the rest and discharge periods [36]. Therefore, after the STc test, the Cr of the subsequent cycle can be retrieved.

4.3. The effects of the controller parameters on the fast charging algorithm

The discussion above, demonstrated that some parameters may play important roles in the fast charging algorithm. In Section 3.2, we noted that the proper selection of the threshold potential represents a trade-off between the charging time and battery health. Herein, Table 5 compares the effects of different threshold potential values on the charging process. Although reducing the threshold potential lowers the safety of the algorithm, this strategy facilitates decreasing the charging time. Indeed, when the threshold potential was reduced from 40 mV to 20 mV, the charging time decreased from 3826 s (63.8 min) to 2579 s (43.0 min), corresponding to a decrease of 32.6%; the charged capacity remained similar. For single-cell charging, a threshold potential of 20 mV might be appropriate. However, the inconsistency of cells in battery pack η_{pack} must be considered. Based on our primary tests, the inconsistency of the anode over-potential is approximately 10 mV; thus, an appropriate threshold potential for battery pack might be 30 mV. Furthermore, the non-uniformity of the current distribution on cell plate η_{cell} must also be considered. The safety margin set for the CCML overshoot and the error of model prediction are denoted as η_{over} and η_{model}, respectively. Without considering the measurement error, a safe value of the threshold potential can be calculated as follows: $\eta_{thr} = \eta_{cell}+\eta_{pack}+\eta_{over}+\eta_{model}$. In this regard, further investigating the anode over-potential distribution within a single cell and the inconsistency among different cells within a battery pack are required to find the optimal values of η_{cell} and η_{pack}.

5. Conclusion

In this paper, a novel non-destructive model-based fast charging algorithm is proposed. The fast charging algorithm can observe the status of the lithium deposition online, which was not previously possible, using a simplified electrochemical model (SP2D). Based on the status of lithium deposition observed by the SP2D model, an online feedback control algorithm for fast charging is further formulated. This algorithm automatically enhances the charging current to keep the observed anode over-potential close to the pre-set threshold potential, thereby decreasing the charging time without harming the battery health.

The fast charging algorithm is first simulated to charge a virtual battery in Comsol. Results showed that 95.3% of the battery capacity could be charged within 10 min and that lithium deposition was successfully suppressed. A large-format commercial lithium-ion battery with a reference electrode is then charged using the fast charging algorithm for experimental validation. The experiment revealed that 96.8% of the battery capacity could be charged within 52.5 min with no lithium deposition at room temperature. Compared with previous fast charging approaches, the proposed algorithm has advantages in both charging speed and safety. The post-mortem analysis and long-term cycling results confirm that the proposed algorithm successfully prevents lithium deposition during fast charging, thereby slowing down the battery aging remarkably. Additionally, the fast charging algorithm can be adaptable for charging from different initial SOCs, making it appropriate for implementation in BMSs. For practical applications, the model parameters were validated through calibration. Then, the controller parameters were adjusted to obtain optimal charging effects. Finally, the algorithm could be used in a BMS, functioning via the real-time transmission of the required current signal to the charger based on the measured voltage response.

Future work based on the proposed fast charging algorithm will address the following topics: (1) fast charging at low temperatures and (2) updating the charging algorithm to consider battery degradation. The charging current must be updating to accommodate the variation in the intrinsic battery properties that occurs during aging. Combined with an appropriate degradation model, the simplified electrochemical model can be utilized for real-time updates.

Acknowledgement

This work is supported by the National Natural Science Foundation of China (Grant No. U1564205), Ministry of Science and Technology of China (Grant No. 2016YES0102200). The first author especially appreciates the technical support by Contemporary Amperex Technology Co., Limited.

References

[1] He H, Xiong R, Guo H. Online estimation of model parameters and state-of-charge of $LiFePO_4$ batteries in electric vehicles. Appl Energy 2012;89:413–20.
[2] Ye Y, Saw LH, Shi Y, Somasundaram K, Tay AA. Effect of thermal contact resistances on fast charging of large format lithium ion batteries. Electrochim Acta 2014;134:327–37.
[3] Park C-K, Zhang Z, Xu Z, Kakirde A, Kang K, Chai C, et al. Variables study for the fast charging lithium ion batteries. J Power Sources 2007;165:892–6.
[4] Hussein AA-H, Batarseh I. A review of charging algorithms for nickel and lithium battery chargers. IEEE Trans Veh Technol 2011;60:830–8.
[5] Klein R, Chaturvedi NA, Christensen J, Ahmed J, Findeisen R, Kojic A. Optimal charging strategies in lithium-ion battery. In: Proceedings of the 2011 American control conference: IEEE; 2011. p. 382–7.
[6] Liu Y-H, Teng J-H, Lin Y-C. Search for an optimal rapid charging pattern for lithium-ion batteries using ant colony system algorithm. IEEE Trans Veh Technol 2005;52:1328–36.

[7] Notten PH, het Veld JO, Van Beek J. Boostcharging Li-ion batteries: a challenging new charging concept. J Power Sources 2005;145:89–94.
[8] Chung S, Andriiko A, Mon'ko A, Lee S. On charge conditions for Li-ion and other secondary lithium batteries with solid intercalation electrodes. J Power Sources 1999;79:205–11.
[9] Sikha G, Ramadass P, Haran B, White RE, Popov BN. Comparison of the capacity fade of Sony US 18650 cells charged with different protocols. J Power Sources 2003;122:67–76.
[10] Li J, Murphy E, Winnick J, Kohl PA. The effects of pulse charging on cycling characteristics of commercial lithium-ion batteries. J Power Sources 2001;102:302–9.
[11] Purushothaman B, Landau U. Rapid charging of lithium-ion batteries using pulsed currents a theoretical analysis. J Electrochem Soc 2006;153:A533–42.
[12] Zou C, Manzie C, Nešić D. PDE battery model simplification for charging strategy evaluation. In: Control conference (ASCC), 2015 10th Asian: IEEE; 2015. p. 1–6.
[13] Pramanik S, Anwar S. Electrochemical model based charge optimization for lithium-ion batteries. J Power Sources 2016;313:164–77.
[14] Suthar B, Ramadesigan V, De S, Braatz RD, Subramanian VR. Optimal charging profiles for mechanically constrained lithium-ion batteries. Phys Chem Chem Phys 2014;16:277–87.
[15] Rahimian SK, Rayman SC, White RE. Maximizing the life of a lithium-ion cell by optimization of charging rates. J Electrochem Soc 2010;157:A1302–8.
[16] Khamar M, Askari J. A charging method for Lithium-ion battery using Min-max optimal control. In: 22nd Iranian Conference on Electrical Engineering (ICEE). Tehran, Iran: IEEE; 2014. p. 1239–43.
[17] Parvini Y, Vahidi A. Maximizing charging efficiency of lithium-ion and lead-acid batteries using optimal control theory. In: Proceedings of the 2015 American Control Conference: IEEE; 2015. p. 317–22.
[18] Guo Z, Liaw BY, Qiu X, Gao L, Zhang C. Optimal charging method for lithium ion batteries using a universal voltage protocol accommodating aging. J Power Sources 2015;274:957–64.
[19] Hu X, Perez HE, Moura SJ. Battery charge control with an electro-thermal-aging coupling. ASME 2015 Dynamic systems and control conference: American Society of Mechanical Engineers; 2015. p. V001T13A2–VT13A2.
[20] Doyle M, Fuller TF, Newman J. Modeling of galvanostatic charge and discharge of the lithium/polymer/insertion cell. J Electrochem Soc 1993;140:1526–33.
[21] Doyle M, Newman J. The use of mathematical modeling in the design of lithium/polymer battery systems. Electrochim Acta 1995;40:2191–6.
[22] Xiong R, Sun F, Chen Z, He H. A data-driven multi-scale extended Kalman filtering based parameter and state estimation approach of lithium-ion polymer battery in electric vehicles. Appl Energy 2014;113:463–76.
[23] Sun F, Xiong R, He H, Li W, Aussems JEE. Model-based dynamic multi-parameter method for peak power estimation of lithium–ion batteries. Appl Energy 2012;96:378–86.
[24] Zhang S, Xu K, Jow T. Study of the charging process of a $LiCoO_2$-based Li-ion battery. J Power Sources 2006;160:1349–54.
[25] Zhang SS. The effect of the charging protocol on the cycle life of a Li-ion battery. J Power Sources 2006;161:1385–91.
[26] Ouyang M, Chu Z, Lu L, Li J, Han X, Feng X, et al. Low temperature aging mechanism identification and lithium deposition in a large format lithium iron phosphate battery for different charge profiles. J Power Sources 2015;286:309–20.
[27] Ouyang M, Feng X, Han X, Lu L, Li Z, He X. A dynamic capacity degradation model and its applications considering varying load for a large format Li-ion battery. Appl Energy 2016;165:48–59.
[28] Yamaki JI, Tobishima SI. Rechargeable lithium anodes. Handbook of Battery Materials, 2nd ed.; 2011. p. 377–404.
[29] Feng X, Weng C, Ouyang M, Sun J. Online internal short circuit detection for a large format lithium ion battery. Appl Energy 2016;161:168–80.
[30] Tippmann S, Walper D, Balboa L, Spier B, Bessler WG. Low-temperature charging of lithium-ion cells part I: Electrochemical modeling and experimental investigation of degradation behavior. J Power Sources 2014;252:305–16.
[31] Han X, Ouyang M, Lu L, Li J. Simplification of physics-based electrochemical model for lithium ion battery on electric vehicle. Part II: Pseudo-two-dimensional model simplification and state of charge estimation. J Power Sources 2015;278:814–25.
[32] Han X, Ouyang M, Lu L, Li J. Simplification of physics-based electrochemical model for lithium ion battery on electric vehicle. Part I: Diffusion simplification and single particle model. J Power Sources 2015;278:802–13.
[33] Arora P, Doyle M, White RE. Mathematical modeling of the lithium deposition overcharge reaction in lithium-ion batteries using carbon-based negative electrodes. J Electrochem Soc 1999;146:3543–53.
[34] Ning G, White RE, Popov BN. A generalized cycle life model of rechargeable Li-ion batteries. Electrochim Acta 2006;51:2012–22.
[35] Liu Y-H, Luo Y-F. Search for an optimal rapid-charging pattern for Li-ion batteries using the Taguchi approach. IEEE Trans Industr Electron 2010;57:3963–71.
[36] Zinth V, von Lüders C, Hofmann M, Hattendorff J, Buchberger I, Erhard S, et al. Lithium plating in lithium-ion batteries at sub-ambient temperatures investigated by in situ neutron diffraction. J Power Sources 2014;271:152–9.